Stimuli-responsive composite biopolymer actuators with selective spatial deformation behavior

Yushu Wang[a,1], Wenwen Huang[b,c,1], Yu Wang[a], Xuan Mu[a], Shengjie Ling[d], Haipeng Yu[e], Wenshuai Chen[e], Chengchen Guo[a], Matthew C. Watson[a], Yingjie Yu[a], Lauren D. Black III[a], Meng Li[a], Fiorenzo G. Omenetto[a], Chunmei Li[a,2], and David L. Kaplan[a,2]

[a]Department of Biomedical Engineering, Tufts University, Medford, MA 02155; [b]Department of Orthopedics of the Second Affiliated Hospital, Zhejiang University School of Medicine, Zhejiang University, Hangzhou 310058, China; [c]The Zhejiang University–University of Edinburgh Institute, Zhejiang University School of Medicine, Zhejiang University, Hangzhou 310058, China; [d]School of Physical Science and Technology, Shanghai Tech University, Shanghai 201210, China; and [e]Key laboratory of Bio-based Material Science and Technology, Ministry of Education, Northeast Forestry University, Harbin 150040, China

Edited by John A. Rogers, Northwestern University, Evanston, IL, and approved May 11, 2020 (received for review February 17, 2020)

Bioinspired actuators with stimuli-responsive and deformable properties are being pursued in fields such as artificial tissues, medical devices and diagnostics, and intelligent biosensors. These applications require that actuator systems have biocompatibility, controlled deformability, biodegradability, mechanical durability, and stable reversibility. Herein, we report a bionic actuator system consisting of stimuli-responsive genetically engineered silk–elastin-like protein (SELP) hydrogels and wood-derived cellulose nanofibers (CNFs), which respond to temperature and ionic strength underwater by eco-friendly methods. Programmed site-selective actuation can be predicted and folded into three-dimensional (3D) origami-like shapes. The reversible deformation performance of the SELP/CNF actuators was quantified, and complex spatial transformations of multilayer actuators were demonstrated, including a biomimetic flower design with selective petal movements. Such actuators consisting entirely of biocompatible and biodegradable materials will offer an option toward constructing stimuli-responsive systems for in vivo biomedicine soft robotics and bionic research.

bionic | stimuli responsive | biopolymers | reversible | actuation

Stimuli-responsive movements of living organisms, from animals (e.g., stroke kinematics of jellyfish, defense mechanisms of invertebrates) to botanical species (e.g., foliage folding of plants), allow such systems to adapt to changes in the environment and provide ample inspiration for novel soft robotics and actuator designs (1–5). Currently, soft actuators with programmable locomotion and rapid environmental response are a focal point in research. Compliance and mechanical properties of soft actuators also make them especially attractive for in vivo medical applications such as drug delivery, surgery, biosensing, and implantable devices (6). Emerging soft actuators are able to complete movements in response to external stimuli, including temperature, pH, humidity, light, and electric/magnetic fields. Among these state-of-the-art actuators, synthetic polymers [e.g., poly(*N*-isopropylacrylamide), poly(*N*,*N*-dimethylaminoethyl methacrylate), poly(ethylene-co-vinyl acetate), and azobenzene polymers], have been most commonly developed as the stimuli-responsive systems (7–14). Additional components of these dynamic systems often include inorganics, such as black phosphorous, graphene oxide, mesoporous silica, and magnetic particles due to their electrochemical, thermal, and optical properties (14–18). Although these materials are accessible, they are difficult to tune due to their inherent physicochemical properties, and thus offer limiting programmable stimuli-responsive properties. Moreover, the majority of these actuators are not useful for in vivo applications due to poor biodegradability, biotoxicity, inefficient actuations in wet environments (19, 20). Therefore, it is attractive to develop intrinsically biocompatible and biodegradable actuators with the capacity for efficient, tunable, and controllable response to external stimuli and complex shape deformation. Such natural, biopolymer-derived actuators would be particularly highly demanded due to the sustainable or ecofriendly material sources, the reusable or degradable options for these devices, and the biocompatibility of such systems when utilized in vivo. With the aim of exploiting an actuator that consists entirely of biocompatible and biodegradable materials and that can be used to recognize the changes of external signals efficiently, we introduced the stimuli-responsive silk–elastin-like proteins (SELPs) as the dynamic unit of the actuator. The genetically engineered SELPs, with the unique combination of silk and elastin domains, can predictably respond to the various stimuli (e.g., temperature, ionic strength, light, pH, glucose, and enzymes, etc.) by tuning the amino acid type located at the position "X" of the elastin domains (GXGVP), yielding a series of proteins with tailored stimuli-responsive characteristics (21–23). Besides that, elastin domains provide elasticity, while hard silk domains (GAGAGS) serve as the mechanical reinforcement motifs (21). Such SELPs constructed by genetic engineering technology exhibit tunable responsiveness by rational design, providing new sources to the families of actuator systems (23).

Sensing and actuation of natural botanic systems are mainly hydration driven (20, 24, 25). For example, the directionality of movements of cone and seed pods are driven by the swelling and de-swelling of cell walls and controlled by anisotropically

Significance

The majority of deformable actuators rely on synthetic materials with stimuli-responsive properties to execute the system, limiting their use in vivo. We designed and built a new class of bionic actuator entirely out of biocompatible and biodegradable materials. Stimuli-responsive genetically engineered silk–elastin-like proteins (SELPs) and cellulose nanofibers (CNFs) are combined to fabricate an actuator system that could effectively respond to physical and chemical stimuli. Programmable and reversible deformations in response to the stimuli have been achieved with this actuator. The SELP/CNF actuator provides an option for fields such as in vivo biomedical soft robotics and biomimetic devices where biocompatibility, biodegradability, biomedical signals recognition, and durability are desired.

Author contributions: Yushu Wang, W.H., X.M., S.L., C.L., and D.L.K. designed research; Yushu Wang, W.H., Yu Wang, X.M., S.L., C.G., M.C.W., Y.Y., and C.L. performed research; Yu Wang, X.M., S.L., H.Y., W.C., C.G., L.D.B., M.L., F.G.O., and C.L. contributed new reagents/analytic tools; Yushu Wang, W.H., Yu Wang, X.M., S.L., H.Y., W.C., C.G., M.C.W., Y.Y., L.D.B., M.L., C.L., and D.L.K. analyzed data; and Yushu Wang, W.H., C.L., and D.L.K. wrote the paper.

The authors declare no competing interest.

This article is a PNAS Direct Submission.

Published under the PNAS license.

[1]Yushu Wang and W.H. contributed equally to this work.

[2]To whom correspondence may be addressed. Email: chunmei.li@tufts.edu or david.kaplan@tufts.edu.

This article contains supporting information online at https://www.pnas.org/lookup/suppl/doi:10.1073/pnas.2002996117/-/DCSupplemental.

First published June 10, 2020.

orientated cellulose fibers (26–28). A well-known example of such systems is the seed dispersal of ice plants through the opening/closure movement of protective valves on the seed pods (Fig. 1*A*). The protective valve opens due to the swelling of cell walls caused by sufficient hydration, which is beneficial to germination of the seeds. In addition, the movements of double-layer plant tissues are programed by highly evolved genetic designs to encode the anisotropic arrangement of cellulose fibers in the cell walls. These sophisticated plant actuation movements are efficient even without the assistance of a nervous system, exploiting the unique structural features and response to environmental stimuli. Such natural strategies can be utilized as a guide to the fabrication of biomimetic soft robotics and microactuation systems with rapid responses and programmable execution. In homage to the wizardry of nature, we present a stimuli-responsive SELP/cellulose nanofiber (CNF) asymmetric bilayer actuator with the capability of imitating similar movements of living organisms with predictability and control. Besides, the biomimetic SELP/CNF actuators with fine-tuning and programmable deformations by rational design have been demonstrated.

Results and Discussion

Design of SELP/CNF Actuators. The components of our systems are all sustainable biopolymers, as shown in Fig. 1*B*. Temperature and ionic strength are the most common physiological signals detected. Herein, the SELP [S_2E_{8R}, block copolymer design with silk (S) domains $(GAGAGS)_2$, and elastin (E) domains with sequence $(GVGVP)_4$ (RGYSLG) $(GVGVP)_3$] that can respond to the changes in temperature and ionic strength was selected. To transform such protein chains into macroscopic materials to mimic the hydration-driven swelling/deswelling phenomenon of plant cell walls, the soft hydrogel with water absorbance property turns out to be an ideal option for the biocompatible actuators (29, 30). SELP hydrogels with high water content undergo significant and reversible changes of volume in response to external stimuli that allow the design of systems with reversible shape transformations. In plant cell walls, the arrangement of cellulose fibers affects the directional movement of plants as mentioned earlier. In addition, due to the thermal stability and chemical inertness, cellulose and its derivatives are potential candidates as passive domains for actuators. Inspired by these principles, CNF-based substrate was utilized as reinforcement and passive phases for our actuator designs.

Here, we adopt an efficient approach to fabricate biomimetic SELP/CNF actuators by using a layer-by-layer construction strategy. Briefly, CNF membranes were prepared via vacuum filtration of CNF suspensions. The SELP hydrogels were rapidly formed by casting mixed SELP/horseradish peroxidase (HRP)/H_2O_2 solutions onto the CNF membranes with the assistance of a polydimethylsiloxane (PDMS) border mold. The PDMS mold was removed after the cross-linking of the SELP hydrogel, to obtain the bilayer structures of the SELP/CNF actuators (Fig. 1*C*). SELP/CNF actuators with performances of reversible shape changes can be attributed to the swelling/deswelling of the SELP hydrogels resulting from water transportation upon triggering with external stimuli of temperature and ionic strength.

Stimuli-Responsive Property of SELP Hydrogels. To translate the protein folding–unfolding upon trigger at the molecular level into reversible and tunable physical property changes at a macroscopic scale, SELP was designed with a tyrosine residue in the elastin blocks to form hydrogels via an enzymatic cross-linking reaction based on HRP (21). SELPs were biosynthesized via seamless cloning strategies and purified via inverse temperature transition cycling. The purified SELPs with molecular weights of ~46.2 kDa were characterized by matrix-assisted laser desorption ionization–time of flight (MALDI-TOF) (*SI Appendix*, Fig. S1). Tyrosine sites of the elastin domains were enzymatically cross-linked by HRP/H_2O_2 reactions to generate the SELP hydrogels using our previously reported procedures (31). Optically transparent SELP hydrogels emitted a luminous blue fluorescence under UV due to the formation of di-tyrosine bonds, a feature absent in the precursor solution (*SI Appendix*, Fig. S2).

Mostly, SELPs are known to undergo a phase transition in aqueous solution upon heating above their lower critical solution temperatures (LCSTs) (32). In order to investigate the stimuli-responsive properties of the SELP hydrogels, ionic strength and temperature stimuli were used to trigger deionized (DI) water-equilibrated hydrogels with a protein concentration of 2.5 wt%. Differential scanning calorimetry (DSC) (Fig. 2*A*) shows that the SELP hydrogels exhibited LCSTs at 15 and 25 °C when submerged in 1 M NaCl solution and DI water, respectively. Meanwhile, the exothermic transition during cooling and heating supported a reversible temperature transition for the SELP hydrogels. Previous work demonstrated that elastin-like proteins

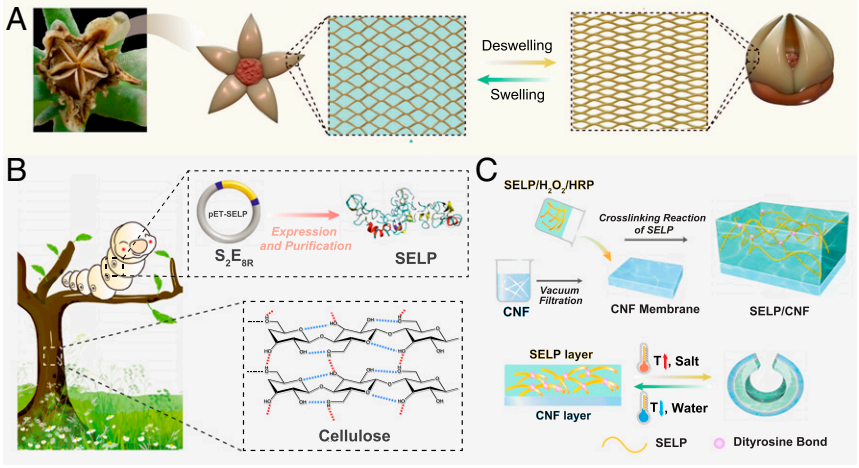

Fig. 1. Design of the bionic actuators. (*A*) Inspiration from the hydration-dependent actuation of ice plant seed capsules. (*B*) Illustration of the genetically engineered SELP and wood-derived cellulose and their molecular structure. (*C*) Schematic diagram of the assembly process of the bilayer SELP/CNF actuators, and the reversible deformation of the actuator under various stimulations.

are soluble in the aqueous solution below the transition temperature, and they undergo a hydrophobic collapse accompanied by a reorientation of water molecules and restructuring of hydrogen bond networks above the transition temperature, resulting in the structural transition to a contracted, aggregated state (33, 34). In the present work, the contraction behavior of SELP hydrogels in DI water and NaCl solutions was observed when the temperature was higher than the corresponding LCSTs (*SI Appendix*, Fig. S3 and Fig. 2*B*). The aggregated SELP molecules in the hydrogels are therefore likely responsible for the shrinking phenomenon. In addition, SELP hydrogels displayed a decreased LCST in NaCl solution, suggesting that the structural folding of SELP molecules is more intense in the aqueous solvent with high ionic strength. Since ions that diffuse into the protein can react with the charged atoms in the peptide chains more strongly, and at the same time, these ions can also promote hydrogen bonds within the peptides. These effects would facilitate the structural transition (35). The thermal-reponsive properties of the SELP hydrogels were further quantitatively studied by recording weight changes when immersed initially in DI water at 4 °C to reach equilibration, followed by immersion in DI water at 60 °C, above the LCST (25 °C). The SELP hydrogels shrunk to about 67.2% of the original weight due to the thermoresponsive properties (*SI Appendix*, Fig. S3). Fig. 2*B* shows that the maximum shrinkage of the SELP hydrogels increased from 75.4 to 92.1% by increasing the concentration of NaCl in solution from 50 mM to 1 M after reaching equilibrium at room temperature. These results confirmed the chemoresponsive capability of these SELP hydrogels. The SELP hydrogels submerged in the NaCl solutions exhibited higher deswelling ratios in comparison with hydrogels triggered by thermal stimulus. The reason is that the ions can promote the structural folding of SELP molecules, thus facilitating the deswelling of the SELP hydrogels (35). Beyond that, the osmotic pressure induced by the NaCl solution also facilitates the contraction of SELP hydrogels. Moreover, a maximum deswelling ratio of 96.5% was observed when the hydrogel was placed in the 500 mM NaCl

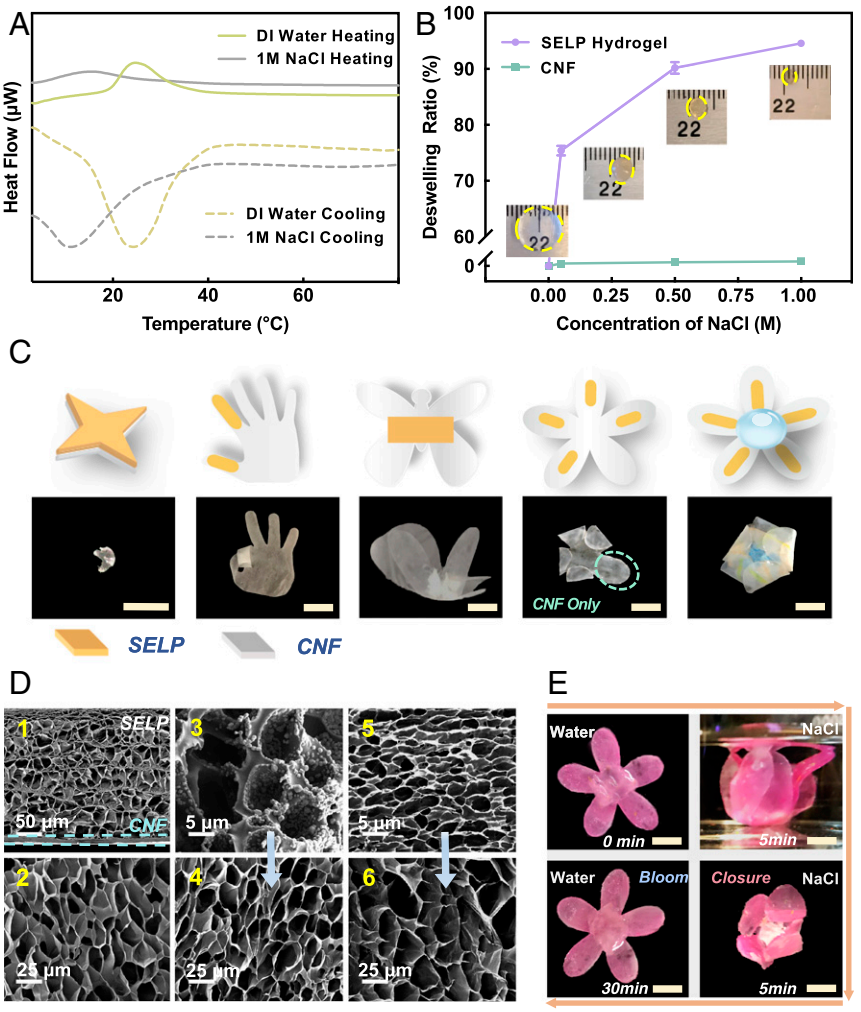

Fig. 2. Characterization of stimuli-responsive SELP hydrogels and actuation of site-selective SELP/CNF actuators. (*A*) DSC heat flow versus temperature curves in DI water and 1 M NaCl, suggesting the stimuli-responsive properties of SELP hydrogels (solid lines and dashed lines represent the heating and cooling processes, respectively). (*B*) Deswelling ratios of the SELP hydrogels and CNF membranes upon exposure in NaCl solutions at room temperature. The *Insets* are the photographs of the SELP hydrogels in swollen states in DI water at 4 °C and the contractive SELP hydrogels immersed in NaCl solutions at room temperature. (*C*) Schematic of 2D predictions, and photographs of 3D programmable SELP/CNF actuators in response to NaCl solution at room temperature. (*D*) SEM images showing the micromorphological changes of (D_1) SELP/CNF bilayer actuators and (D_2) SELP hydrogels in swollen states at 4 °C DI water, SELP hydrogels in contracted states at (D_3) 1 M NaCl solutions at room temperature and (D_5) 60 °C DI water, respectively, and (D_4 and D_6) equilibrated back to 4 °C DI water of (D_3 and D_5), indicating the reversibility after exposure to stimuli. (*E*) One cycle of biomimetic closure–bloom movement of flower-shaped SELP/CNF actuators. (Scale bars: *C* and *E*, 10 mm.)

solution at 37 °C, indicating the dual (salt, temperature) stimuli-responsive features of the SELP hydrogels (*SI Appendix*, Fig. S4). The dual stimuli-responsive features of SELP hydrogels were characterized by dynamic mechanical analysis. Viscoelastic properties, including storage and loss modulus of the SELP hydrogels, were measured in water at various temperatures and in 1 M NaCl solution. An increase of hydrogel stiffness was observed when the temperature was above the LCST or treated in the NaCl solutions, due to the deswelling properties (*SI Appendix*, Fig. S5).

The cyclic stimuli (temperature and ionic strength)-triggered volumetric changes of the SELP hydrogels were evaluated after switching the external solvent from the stimulus conditions (including DI water at 60 °C and 500 mM NaCl solution at room temperature and 37 °C) to the reverse conditions (e.g., DI water at 4 °C) for more than 10 cycles (*SI Appendix*, Figs. S6 and S7). The deswelling ratios were relatively constant over these repetitive temperature and ionic strength cyclic stimulations, suggesting that the thermal and ionic strength responses of the SELP hydrogels were reversible and reproducible. The SELP hydrogels in NaCl solutions achieved maximum deswelling over about 20 min compared with the thermal stimulation process, which takes around 40 min in DI water at 60 °C. However, all of the contracted SELP hydrogels returned nearly to their original size when equilibrated back to 4 °C in DI water for ∼30 min. The changes in the molecular structure of SELP hydrogels upon application and removal of the external stimulus were assessed by Fourier transform infrared spectroscopy (FTIR) (*SI Appendix*, Fig. S8). The percentages of secondary structures were calculated by fitting the Fourier self-deconvoluted amide I peak using a previously published method (36). FTIR analysis indicated that the percentage of random coil decreased, and the percentage of β-turn increased when the temperature or ionic strength was increased. The percentages of random coil and β-turn almost returned to their original values after the stimulus was removed. This reversible structural change is the main driving force that causes the reversible contraction of the top SELP layer. In addition, the absence of absorbance peak in the region of 1,624 cm^{-1} representing the presence of β-sheets suggested that there was no irreversible ordered secondary structure formation. This finding also supports the explanation of the reversibility of the SELP hydrogels.

Stimuli-Responsive Actuation of SELP/CNF Actuators. CNF suspensions were prepared from the ultrasonic treatment of wood cellulose pulps to form nanofiber bundles with diameters of several hundred nanometers, as previously reported (37). After vacuum filtration of the CNF suspension, translucent CNF membranes were formed with three-dimensional (3D) interwoven network structures (*SI Appendix*, Fig. S9 *A* and *B*). The intrachain and interchain hydrogen bonded networks on the surface of the CNF bundles endowed the CNF membranes with flexible and tough mechanical properties, critical for repetitive folding and actuation (*SI Appendix*, Fig. S9*C*). Furthermore, in contrast to the SELP hydrogels, the CNF membranes maintained their original size when immersed in NaCl solutions and DI water at 60 °C, thus serving as the passive component for the bilayer systems (Fig. 2*B* and *SI Appendix*, Fig. S10).

SELP/CNF bilayer actuators capable of complex deformations were achieved via a selective local cross-linking reaction (*SI Appendix*, Fig. S11). CNF membranes were tailored into specific shapes, and covered with various shapes of PDMS molds at specific positions on their surfaces. Mixed SELP/HRP/H_2O_2 solutions were added into the PDMS molds, resulting in the formation of SELP hydrogels with specific shapes at the contact location due to the rapid cross-linking reaction. The stimuli-responsive SELP hydrogels with reversible swelling/deswelling properties were employed as the active domains in these bilayer designs. The natural tendency was for the bilayer systems with asymmetric volumetric changes to bend toward the SELP side of the bilayer upon stimulation due to coalescence of the active layer. Thus, the site-specific deposition of SELP hydrogels can be used as localized "hinges" to control where folds were formed. The performance of these SELP/CNF actuators was qualitatively estimated preliminarily by fabricating simple models with biomimetic patterns and using the stimulus of exposure to 1 M NaCl solution at room temperature. Various 3D origami-like geometries were obtained, such as claws, fingers, butterflies, and petals of flowers (Fig. 2*C*) guided by the localized bend of hinge regions and designed to mimic shapes found in nature. The movements, like grasping, bending, lifting, and packaging, were employed by taking advantage of the site-specific deposition and deswelling of the SELP hydrogel components. In general, the final structure of the models was mainly determined by the location of the SELP hydrogels on the surface of the CNF layer and the shapes of the CNF utilized. This series of programmable actuations induced by predictive designs demonstrated the potential to control selective mechanical motility with complex structures.

The structure of the SELP/CNF bilayers and the structural transformations in SELP hydrogels upon stimuli were characterized by scanning electron microscopy (SEM) (Fig. 2*D*). The cross-sectional SEM images of water equilibrated SELP/CNF bilayer actuators display an enlarged interface to confirm that the SELP hydrogel was intimately associated with and infused with the underlying CNF membrane during the enzymatic cross-linking reactions (Fig. 2 *D*, panel 1 and *SI Appendix*, Fig. S12). The conditions for enzymatic cross-linking reaction were controlled so that the gelation occurred rapidly to avoid excessive infiltration of the SELPs into the CNS layer yet to ensure efficient binding between the two layers. This fabrication approach supported the functional integrity of the materials and avoided delamination during actuation. The SELP hydrogels with interconnected porous network structures also served as reservoirs for water to support sufficient hydraulic transport (Fig. 2 *D*, panel 2). The coalesced aggregated structures of the SELP layers were observed after exposure to 1 M NaCl solution and DI water at 60 °C due to water desorption (Fig. 2 *D*, panels 3 and 5). The morphology of the SELP layers almost recovered to its original state when reequilibrated in DI water at 4 °C (Fig. 2 *D*, panels 4 and 6). The reversible actuating performance of the SELP/CNF system was demonstrated by actuators consisting of flower-shaped CNF membranes stained with waterproof dyes and a SELP hydrogel located at the center of the membrane (Fig. 2*E*). The bionic closing–blooming movements of these flower-shaped actuators were achieved by placement into 1 M NaCl solution and then back into DI water at 4 °C for 30 min, harnessing the reversible swelling/deswelling properties of the SELP hydrogels.

The actuation performance of these SELP/CNF bilayers with the typical rectangular shape of 1 × 6 mm was evaluated in response to the changes of temperature and ionic strength. The bilayer actuators bent toward the SELP side upon stimulation due to the asymmetric volumetric changes in the two layers, forming a bent arch with a curvature radius of r. The bending curvature (i.e., $1/r$) of the bilayer actuators was controlled by changing the thickness ratio of the active SELP layer to the passive CNF layer. The thickness ratios could be tuned by varying the thicknesses of the CNF layer while keeping the thickness of SELP layer constant (*SI Appendix*, Fig. S13). The bending curvature of SELP/CNF bilayers was significantly affected by the thickness ratio. In Fig. 3*A*, the experimental data show that the curvature of SELP/CNF bilayers increased with the thickness ratio. These results were supported by the modified Timoshenko bimetallic thermostats theory, which can be used to predict the relationship between the thickness ratio and curvature of bilayers when consisting of distinct materials (5, 20, 28, 38, 39):

$$\frac{1}{r} = \frac{6\varepsilon(1+m)^2}{h\left(3(1+m)^2 + (1+mn)\left(m^2 + \frac{1}{mn}\right)\right)},$$

where E and h are the elastic moduli and the thickness of the layers, respectively; h is the total thickness ($h = h_{SELP} + h_{CNF}$), $n = E_{SELP}/E_{CNF}$, $m = h_{SELP}/h_{CNF}$; and ε is the difference in expansion coefficient between the two layers. In the present work, ε corresponds to the volumetric contraction difference between the two layers upon NaCl stimulation. The elastic modulus of SELP hydrogels was calculated as 288 Pa based on the contraction force measurements (*SI Appendix*, Fig. S14), while the tensile Young's modulus of the CNF layer was ~0.71 MPa (*SI Appendix*, Fig. S15). The experimental values fit well with the theoretical values, especially for bilayers with SELP/CNF thickness ratios less than 10. The larger deviation between the experimental and theoretical values at thickness ratio of 10 is probably due to the larger deformations of the SELP/CNF actuators, which are not well accounted for in the theoretical models (Fig. 3*A*). Additionally, to investigate the upper limit of the bending behavior, the maximum diameter changes (MDCs) were defined to evaluate the extent of deformation of the SELP/CNF actuators with various thickness ratios (*SI Appendix*, Fig. S16*A*), followed by exposure of these strips to NaCl solutions with varying concentrations at room temperature (Fig. 3*B*). The MDC of all actuators increased with increasing salt concentration from 0.5 to 500 mM, and the MDC of actuators with thickness ratio of 10 reached 90.4% in the 500 mM NaCl solution. These results suggested that the MDC of the bilayer actuators was proportional to the amount of SELP hydrogel and concentration of the NaCl solution, but with an inverse relationship with the thickness of the CNF membrane. Furthermore, Fig. 3*C* shows the actuation time of the SELP/CNF actuators with thickness ratio of 10, where more than 80% of the shape change occurred within 10 min. The *Insets* in Fig. 3*C* are photographs of the bending of SELP/CNF strips at different actuation times. Over time, the degree of deformation increased. Such rectangle strips gradually bent to the upper limit and deformed to the coiled shapes with tight curvatures. Fig. 3*D* confirmed the reversible actuation movement of SELP/CNF strips with thickness ratio of 10 during continuous changes of NaCl concentration from 0 to 500 mM over 100 cycles. The shape transformations were completely reversible, and the constant amplitude curve during the shape-relaxation actuation of the MDC is shown after each stimulation cycle, again demonstrating good stability and reversibility of the SELP/CNF actuators. In addition, the reversible movement of actuators switched from the 500 mM NaCl to 4 °C DI water was revealed by SEM analysis, and the strongly attached bilayers were observed during cycles (*SI Appendix*, Fig. S16 *B–E*). The similar scenarios of the SELP/CNF actuators as in the preceding discussion were also performed by varying the temperature of the DI water. The MDC of the SELP/CNF strips with thickness ratio of 10 was positively related to the temperature (*SI Appendix*, Fig. S17*A*). The *Insets* in the SEM image exhibit the curved SELP/CNF strips upon exposure to water at 60 °C, and the bending strips eventually straighten back to their initial state when cooled in the water at 4 °C (*SI Appendix*, Fig. S17*B*).

Programmable Actuation of Multilayer SELP/CNF Actuators. Inspired by the closure movements of flora, we generated biomimetic multilayer actuators to achieve programmable and complex actuation by employing the SELP/CNF system. The original structure of the multilayer actuator was composed of six layers of alternating petal-shaped CNF membranes as the passive domains and SELP hydrogels as the active domains. Similar to the selective local crosslinking reaction above, three petal-shaped CNF membranes with descending petal sizes were prepared, and a specific volume of the

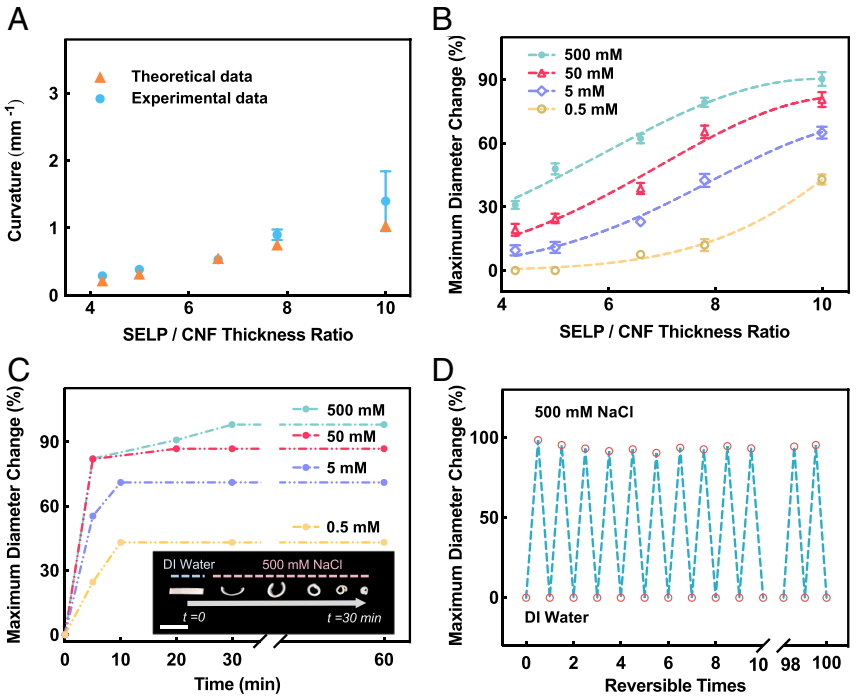

Fig. 3. Quantitative analysis of the stimuli-responsive SELP/CNF bilayer actuators. (*A*) Bending curves for the bilayer strip actuators depending on the thickness ratio of the SELP to the CNF layer in 0.5 M NaCl solutions at room temperature. (*B*) MDC curves of the bilayer strip actuators with various thickness ratios, and (*C*) MDC versus time curves of bilayer strip actuators with thickness ratio of 10 in response to 0.5, 5, 50, and 500 mM NaCl solutions at room temperature, respectively. The *Insets* are photographs of bending strip actuators at the corresponding time points. (Scale bar, 5 mm.) (*D*) Cyclic stability of the MDC of the bilayer strip actuators with thickness ratio of 10 under stimuli changes from 4 °C DI water to NaCl solutions at room temperature.

SELP hydrogel was cross-linked above the center of each CNF membrane, respectively. Then, three SELP/CNF bilayer units were stacked together in a vertical fashion to form the six-layer structures by exploiting the viscosity of the SELP hydrogels. The area of the SELP hydrogel covered on each layer of CNF membrane was adjusted by varying the volume of the mixed SELP/HRP/H_2O_2 solution and confined within the circular PDMS molds (Fig. 4*A*). As the degree of contraction of the SELP hydrogels increased in response to the 1 M NaCl solutions over time, the CNF layer gradually bent to its limit in 20 min. In the present actuator design, the resultant bending directions and final bending angles of the CNF layer were constrained by the location and area ratios covered by the SELP hydrogels. With the increase of coverage in terms of area ratios from the bottom to the top layer, the bending angles of the CNF layer increased, and the maximum bending angle of the top CNF layer reached ∼90° (Fig. 4*A*, *SI Appendix*, Fig. S18, and Movie S1). Finally, the area ratios of each petal-shaped CNF layer covered by the SELP hydrogels could be finely tuned, ultimately obtaining a bionic flower shaped actuator. Furthermore, finite element simulations (finite element analyses [FEAs]) were performed to predict the shape morphing of the assembled structures. The design of a 3D FEA model was based on the actual geometrical configuration (Fig. 4*B*). Similar to the experimental data, the magnitudes of bending angles of the CNF layers were relevant to the structural configurations resulting from the extent of contraction of the SELP hydrogels processed at different time points and the area ratio covered by the SELP hydrogels. As a result, the combination of experimental data and simulation approach confirmed that the biomimetic SELP/CNF actuators could be programmed by rational design.

Conclusions

In summary, learning from the hydration-driven botanic systems, we presented a stimuli-responsive actuator built from rationally designed genetically engineered SELP and CNF. The biocompatible SELP/CNF actuators take advantage of the characteristic of the SELP hydrogels that can respond to the changes in temperature and ionic strength, supporting intricate morphological transformations via prepatterned control of the materials assembly. Quantitative analysis of the final geometry allowed for predictions of deformation when trigged with stimuli, thus the ability to fine-tune actuators and shape changes of the structures. Stable reversible deformations and durability of SELP/CNF actuators were further demonstrated. Moreover, inspired by the motions from living organisms, biomimetic actuator movements (e.g., multilayer petals blooming and their closure) were achieved. Genetically engineered proteins with tunable stimuli-responsive properties are used as the dynamic unit to fabricate the deformable actuators. A series of diverse stimuli-triggered actuators that can respond to light, pH, glucose, and enzyme signals should also be feasible by incorporating sequences based on the SELPs library we previously developed (21, 22). We anticipate that such biocompatible actuators can provide an avenue to customized responsiveness toward applications for in vivo biomedical soft robotics and bionic devices.

Materials and Methods

Expression and Purification of SELP and CNF. All chemicals were purchased from Sigma-Aldrich or Fisher Scientific, unless otherwise noted, and were used as received. The expression, production, and purification of the SELPs were performed according to our previous work (21). Briefly, the multimer genes SELP [$(GAGAGS)_2$ $(GVGVP)_4$ (RGYSLG) $(GVGVP)_3$] were inserted into the pET-19b3 expression vector in *Escherichia coli* strain BL21Star (DE3) (Invitrogen). For the production and purification of SELP, the recombinant strains were grown in 500-mL flasks containing 100 mL of Luria–Bertani medium for overnight culture in a shaking incubator at 250 rpm, 37 °C. A 100-mL seeding culture was transferred to 2 L of yeast extract medium for fermentation at 37 °C. Cells were induced with 1 mM isopropyl-β-D-thiogalactopyranoside when the optical density at 600 nm reached ∼10. After 6-h induction, cells were harvested by centrifugation at 8,000 rpm for 15 min at 4 °C. SELPs were purified using the inverse temperature cycling method. The

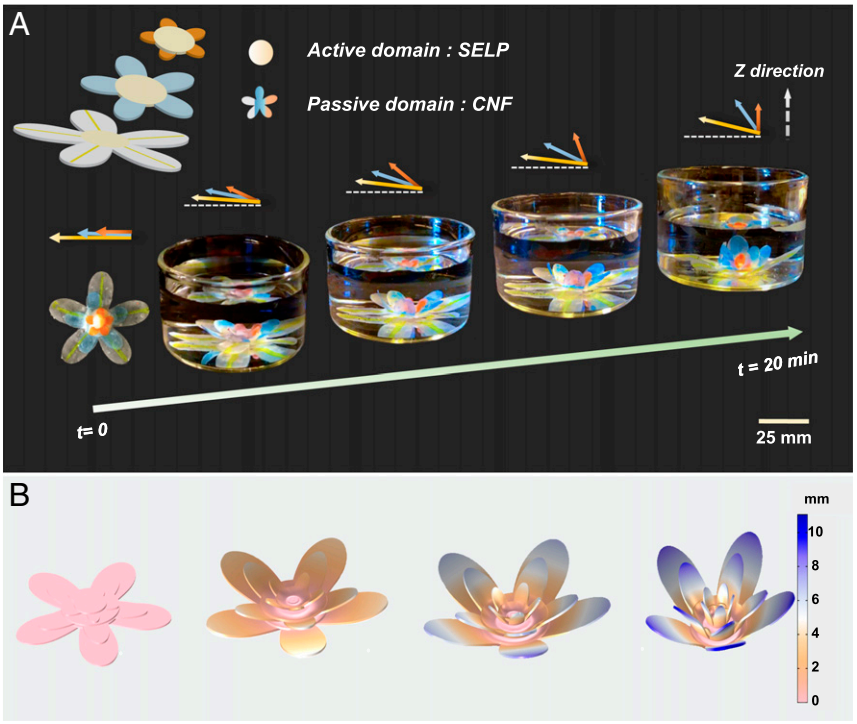

Fig. 4. Biomimetic multilayer SELP/CNF actuators. (*A*) Schematic of the structure designs and the photographs of the transformation process of the petal-shaped actuators over time in 1 M NaCl solutions at room temperature. The color of actuators was stained by waterproof inks. (*B*) Result of COMSOL simulation.

bacterial pellet was resuspended in PBS with lysozyme, and the cells were dispersed by sonication on ice. The cell lysate was cleared by centrifugation at 8,000 rpm for 15 min at 4 °C, and then the supernatant containing SELP was diluted by 2× TN buffer, incubated at 70 °C for 2 h, and centrifuged at 5,000 rpm for 3 min at 40 °C. The supernatant was then discarded, and the pellet containing SELP was recovered by DI water at 4 °C overnight followed by another cold spin at 8,000 rpm for 15 min at 4 °C. The supernatant containing the purified SELP was dialyzed (MWCO, 3.5 kDa) against DI water for 24 h. The purity of the protein was determined by MALDI-TOF (Bruker Corporation). The yield of lyophilized SELPs was ∼1 g of purified protein per liter of culture medium. The CNFs were derived from poplar wood according to our reported methods (37). The purified cellulose suspensions were nanofibrillated by a Branson 450 Sonifier (Branson Ultrasonics Company) at 40% amplitude with interval of 10 s for 30 min to generate a 0.5 wt% wood CNF suspension.

Preparation of Cross-Linked SELP Hydrogels and CNF Membranes. SELP hydrogels were prepared using an enzymatic cross-linking method (21). The lyophilized SELP powder was dissolved in DI water at 4 °C for 4 h to form a SELP solution. HRP, type VI (Sigma-Aldrich), powder was mixed with DI water to form a 40 mg·mL^{-1} with a concentration of 10,000 U·mL^{-1} HRP stock solution. To fabricate a 2.5 wt% SELP hydrogel, 10 μL of 0.1 wt% hydrogen peroxide (H_2O_2) solution was added into 250 μL, 2.5 wt% SELP solution, for a final concentration of 1.1 mM and then a 5 μL HRP stock solution was added into SELP/H_2O_2 mixture solution (200 U HRP/mL SELP) to initiate the cross-linking reaction. The reaction mixture was mixed by gentle shaking to initiate gelation and incubated overnight at 4 °C. Homemade PDMS molds with various patterns were prepared using a laser cutter. CNF membranes were fabricated by vacuum filtration of the CNF dispersions through a Sigma-Aldrich vacuum filtration assembly, which was covered with a commercial polycarbonate filtration membrane (pore size, 0.2 μm). The thickness of the as-prepared CNF membranes, for example, with diameters of 16 mm could be tuned by changing the volume of the 0.5 wt% CNF dispersions (e.g.,700, 900, 1,000, and 1,500 μL) used.

Preparation of SELP/CNF Actuators. To fabricate selective local cross-linking SELP/CNF actuators, well-mixed SELP/HRP/H_2O_2 solutions were poured into the PDMS molds covering the surface of the patterned CNF membranes. It should be noted that the primary cross-linking process of SELP hydrogels completed in several seconds. After complete cross-linking for 12 h at 4 °C, the PDMS molds were easily separated. Additionally, staining with waterproof inks was used for imaging CNF membranes with a digital camera. For the fabrication of SELP/CNF strip actuators, 250 μL of well-mixed SELP/HRP/H_2O_2 solutions were rapidly cast onto the CNF membranes with the help of a circular PDMS mold with the diameter of 16 mm. After complete cross-linking for 12 h at 4 °C, the PDMS molds were removed, and the bilayer SELP/CNF actuators were immersed into DI water overnight to remove residue reagents. SELP/CNF bilayer strips with dimensions of 10-mm length and 6-mm width were tailored for the assessment of actuation performance. For the fabrication of six-layer SELP/CNF petal-shaped actuators, we first cut CNF membranes into the shape of petals with the outer diameter sizes of 50, 32, and 17 mm, and 255, 255, and 80 μL of well-mixed SELP/HRP/H_2O_2 solutions were rapidly cast onto the three petal-shaped CNF membranes correspondingly to carry out the cross-linking reaction with the assistance of the circular PDMS molds with the diameter of 16, 16, and 10 mm. The three petal-shaped SELP/CNF actuators with descending petal sizes from the bottom to top were stacked together with the vertical fashion due to the viscosity of the SELP hydrogels sandwiched between the middle layers of the six-layer structure.

Detailed material characterizations are shown in *SI Appendix*.

Data Availability. All relevant data are included herein or in *SI Appendix*.

ACKNOWLEDGMENTS. We thank the Army Research Office (Grant W911NF-17-1-0384), NIH (Grants P41EB002520 and U01EB014976), and Fundamental Research Funds for the Central Universities (K20200099) for support of this work. Yushu Wang acknowledges the financial support from China Scholarship Council. We thank Dr. Erica Kemmerling at Tufts University for helpful suggestions.

1. M. Wehner *et al.*, An integrated design and fabrication strategy for entirely soft, autonomous robots. *Nature* **536**, 451–455 (2016).
2. J. C. Nawroth *et al.*, A tissue-engineered jellyfish with biomimetic propulsion. *Nat. Biotechnol.* **30**, 792–797 (2012).
3. J. R. Capadona, K. Shanmuganathan, D. J. Tyler, S. J. Rowan, C. Weder, Stimuli-responsive polymer nanocomposites inspired by the sea cucumber dermis. *Science* **319**, 1370–1374 (2008).
4. W. Fan *et al.*, Dual-gradient enabled ultrafast biomimetic snapping of hydrogel materials. *Sci. Adv.* **5**, eaav7174 (2019).
5. A. S. Gladman, E. A. Matsumoto, R. G. Nuzzo, L. Mahadevan, J. A. Lewis, Biomimetic 4D printing. *Nat. Mater.* **15**, 413–418 (2016).
6. M. Cianchetti, C. Laschi, A. Menciassi, P. Dario, Biomedical applications of soft robotics. *Nat. Rev. Mater.* **3**, 143–153 (2018).
7. L. Hines, K. Petersen, G. Z. Lum, M. Sitti, Soft actuators for small-scale robotics. *Adv. Mater.* **29**, 1603483 (2017).
8. S. Wei *et al.*, Bioinspired synergistic fluorescence-color-switchable polymeric hydrogel actuators. *Angew. Chem. Int. Ed. Engl.* **58**, 16243–16251 (2019).
9. B. Jin *et al.*, Programming a crystalline shape memory polymer network with thermo- and photo-reversible bonds toward a single-component soft robot. *Sci. Adv.* **4**, eaao3865 (2018).
10. M. Behl, K. Kratz, U. Noechel, T. Sauter, A. Lendlein, Temperature-memory polymer actuators. *Proc. Natl. Acad. Sci. U.S.A.* **110**, 12555–12559 (2013).
11. S. Zhang *et al.*, A pH-responsive supramolecular polymer gel as an enteric elastomer for use in gastric devices. *Nat. Mater.* **14**, 1065–1071 (2015).
12. J. Cao *et al.*, Arbitrarily 3D configurable hygroscopic robots with a covalent-noncovalent interpenetrating network and self-healing ability. *Adv. Mater.* **31**, e1900042 (2019).
13. J. Chen *et al.*, Artificial muscle-like function from hierarchical supramolecular assembly of photoresponsive molecular motors. *Nat. Chem.* **10**, 132–138 (2018).
14. G. Wu *et al.*, High-performance hierarchical black-phosphorous-based soft electrochemical actuators in bioinspired applications. *Adv. Mater.* **31**, e1806492 (2019).
15. B. Han *et al.*, Plasmonic-assisted graphene oxide artificial muscles. *Adv. Mater.* **31**, e1806386 (2019).
16. R. K. Kramer, C. Majidi, R. J. Wood, Masked deposition of gallium-indium alloys for liquid-embedded elastomer conductors. *Adv. Funct. Mater.* **23**, 5292–5296 (2013).
17. W. Hu, G. Z. Lum, M. Mastrangeli, M. Sitti, Small-scale soft-bodied robot with multimodal locomotion. *Nature* **554**, 81–85 (2018).
18. D. Rus, M. T. Tolley, Design, fabrication and control of soft robots. *Nature* **521**, 467–475 (2015).
19. H. Shahsavan *et al.*, Bioinspired underwater locomotion of light-driven liquid crystal gels. *Proc. Natl. Acad. Sci. U.S.A.* **117**, 5125–5133 (2020).
20. L. Ionov, Biomimetic hydrogel-based actuating systems. *Adv. Funct. Mater.* **23**, 4555–4570 (2013).
21. W. Huang *et al.*, Design of multistimuli responsive hydrogels using integrated modeling and genetically engineered silk-elastin-like proteins. *Adv. Funct. Mater.* **26**, 4113–4123 (2016).
22. Q. Wang *et al.*, High throughput screening of dynamic silk-elastin-like protein biomaterials. *Adv. Funct. Mater.* **24**, 4303–4310 (2014).
23. W. Huang *et al.*, Synergistic integration of experimental and simulation approaches for the de novo design of silk-based materials. *Acc. Chem. Res.* **50**, 866–876 (2017).
24. W. G. van Doorn, U. Van Meeteren, Flower opening and closure: A review. *J. Exp. Bot.* **54**, 1801–1812 (2003).
25. J. M. Skotheim, L. Mahadevan, Physical limits and design principles for plant and fungal movements. *Science* **308**, 1308–1310 (2005).
26. R. M. Erb, J. S. Sander, R. Grisch, A. R. Studart, Self-shaping composites with programmable bioinspired microstructures. *Nat. Commun.* **4**, 1712 (2013).
27. R. Elbaum, L. Zaltzman, I. Burgert, P. Fratzl, The role of wheat awns in the seed dispersal unit. *Science* **316**, 884–886 (2007).
28. M. J. Harrington *et al.*, Origami-like unfolding of hydro-actuated ice plant seed capsules. *Nat. Commun.* **2**, 337 (2011).
29. J. D. Ehrick *et al.*, Genetically engineered protein in hydrogels tailors stimuli-responsive characteristics. *Nat. Mater.* **4**, 298–302 (2005).
30. C. M. Gomes, C. Liu, J. A. Paten, S. M. Felton, L. F. Deravi, Protein-based hydrogels that actuate self-folding systems. *Adv. Funct. Mater.* **29**, 1805777 (2019).
31. B. P. Partlow *et al.*, Highly tunable elastomeric silk biomaterials. *Adv. Funct. Mater.* **24**, 4615–4624 (2014).
32. J. Yeo *et al.*, Unraveling the molecular mechanisms of thermo-responsive properties of silk-elastin-like proteins by integrating multiscale modeling and experiment. *J. Mater. Chem. B.* **6**, 3727–3734 (2018).
33. A. Tarakanova *et al.*, Modeling and experiment reveal structure and nanomechanics across the inverse temperature transition in *B. mori* silk-elastin-like protein polymers. *ACS Biomater. Sci. Eng.* **3**, 2889–2899 (2017).
34. K. B. Rembert *et al.*, Molecular mechanisms of ion-specific effects on proteins. *J. Am. Chem. Soc.* **134**, 10039–10046 (2012).
35. A. Tarakanova, W. Huang, A. S. Weiss, D. L. Kaplan, M. J. Buehler, Computational smart polymer design based on elastin protein mutability. *Biomaterials* **127**, 49–60 (2017).
36. W. Huang, S. Krishnaji, X. Hu, D. Kaplan, P. Cebe, Heat capacity of spider silk-like block copolymers. *Macromolecules* **44**, 5299–5309 (2011).
37. Y. Wang *et al.*, Wood-derived nanofibrillated cellulose hydrogel filters for fast and efficient separation of nanoparticles. *Adv. Sustainable. Syst.* **3**, 1900063 (2019).
38. S. Timoshenko, Analysis of bi-metal thermostats. *J. Opt. Soc. Am.* **11**, 233–255 (1925).
39. J. Mu *et al.*, Molecular-channel driven actuator with considerations for multiple configurations and color switching. *Nat. Commun.* **9**, 590 (2018).